J. Phys. B: At. Mol. Opt. Phys. **41** (2008) 074019 (7pp) doi:10.1088/0953-4075/41/7/074019

Modelling of ultrafast coherent strong-field dynamics in potassium with neural networks

R Selle[1,2], T Brixner[1,2], T Bayer[3], M Wollenhaupt[3] and T Baumert[3]

[1] Physikalisches Institut, Universität Würzburg, Am Hubland, 97074 Würzburg, Germany
[2] Institut für Physikalische Chemie, Universität Würzburg, Am Hubland, 97074 Würzburg, Germany
[3] Institut für Physik und CINSaT, Universität Kassel, Heinrich-Plett-Strasse 40, 34132 Kassel, Germany

E-mail: brixner@phys-chemie.uni-wuerzburg.de

Received 1 October 2007, in final form 7 February 2008
Published 25 March 2008
Online at stacks.iop.org/JPhysB/41/074019

Abstract
We investigate the applicability of neural networks (NNs) for the automated generation of effective computer models for coherent light–matter interactions. The simulation of Autler–Townes doublets from strong-field ionization of potassium atoms is chosen as a test system that exhibits distinct quantum-mechanical effects. Shaped femtosecond laser pulses are employed for studying the response of a quantum-mechanical system to a large variety of different electric fields, and the resulting data can be used for training a NN. We show that a NN is able to approximate the investigated process in parameter regions sampled by the training data and that it can be employed for the interpolation of control landscapes.

(Some figures in this article are in colour only in the electronic version)

1. Introduction

Despite the considerable increase in computing power, *ab initio* calculations, e.g., for the prediction of light–matter interactions remain limited to small molecular systems to date. However, information on this interaction may be extracted directly from experimental data. In this context, the manipulation of light fields with femtosecond laser pulse shapers [1] opens up new possibilities, as the ability for almost-arbitrary field tailoring provides us with an opportunity for testing the response of quantum systems with respect to a large number of different electromagnetic fields. Thus it should be possible to obtain a significant amount of information not available with ordinary, unshaped laser pulses. However, the question arises of how to process these data, i.e., which pulse shapes should be employed, and by which means the complex system response can be evaluated in a general fashion.

While optimization schemes such as evolutionary algorithms or simulated annealing are well suited for finding the best laser pulse shape according to a specific optimization objective in quantum control scenarios [2–13], they are not designed for and are not capable of evaluating the system's responses in a systematic fashion. Hence other methods might be better suited for the specific purpose of analysing light-driven quantum-mechanical processes. In this case, the objective of such methods should not be to optimize a certain quantum-mechanical process or to reach user-specified quantum states, but rather to obtain some kind of model for the system response to applied light fields. Neural networks (NNs) [14, 15] can be employed for the automated generation of approximated input–output maps, and we have recently introduced them for the modelling of simple test systems, namely second harmonic generation (SHG) and molecular fluorescence [16].

In this contribution, we study the applicability of NNs to predict photoelectron spectra from strong-field ionization of potassium atoms. The potassium atom, irradiated by an intense femtosecond laser field, represents a fully coherent system, i.e., no decoherence mechanisms are operative on the interaction time scale, and thus the quantum-mechanical phase is well defined and preserved. As described in section 2, the process considered here is based on a REMPI-type (resonance-enhanced multiphoton ionization) excitation scheme. However, unlike conventional REMPI schemes, which usually are related to the weak-field regime, excitation by strong laser fields will effectively induce population

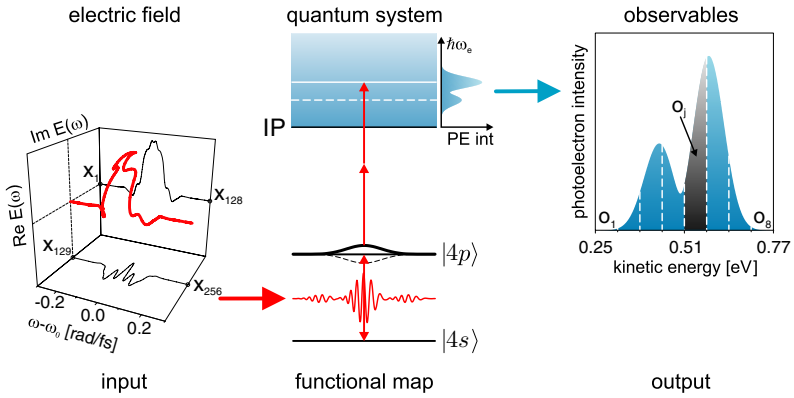

Figure 1. Schematic of the input–output map for the physical model system. The quantum system, i.e., the potassium atom (centre), comprises the two-level system |4s⟩–|4p⟩ (thin black lines) coupled to an ionic continuum. Interaction with an intense shaped femtosecond laser field displayed in the frequency domain (left) yields energy-resolved photoelectron spectra (right). With regard to the NN, a suitable representation of the laser electric field, taken at discrete sampling points x_i, serves as an input for the NN to model the quantum system. The resulting photoelectron spectrum, sampled at a finite number of energy intervals o_j, represents an output, with the laser–atom interaction providing a functional input–output map.

depletion and Rabi-cycling within the resonant subsystem. REMPI excitation of coherent systems in strong laser fields provides an ideal test bed to evaluate the performance of NNs in approximating the response of coherent quantum-mechanical systems. In general, the dynamics of the potassium atom induced by shaped strong laser fields will depend critically on all details of the laser pulse such as the pulse energy, the pulse envelope, the instantaneous frequency and phase jumps. Strong-field ionization of potassium atoms by resonant, shaped laser fields has been studied recently [17]. It was pointed out that the control mechanism at play in the light–atom interaction is the selective population of dressed states (SPODS) [18–21]. Besides the sensitivity to the pulse shape—as exemplified by variations of the absolute pulse intensity as well as the relative intensities of pulses within a sequence [21, 22]—SPODS critically depends on variations of the optical phase. The influence of changes in the instantaneous frequency has been demonstrated using chirped pulses [20] and was discussed in terms of rapid adiabatic passage (RAP) [23]. Likewise, discrete temporal phase jumps are capable of realizing SPODS with high efficiency as was demonstrated by the use of double pulses and multipulse sequences [21, 22]. In this case, the physical mechanism is based on photon locking (PL) [24, 25]. Together with the nonlinearity of the photoelectron signal due to the multi-photon ionization step, the prediction of photoelectron spectra for a given input electric field is a complex and challenging task for a NN.

The pulse-shaping experiment shown schematically in figure 1 can be interpreted in the following way: the electric field of the shaped laser pulse serves as an input to the investigated quantum system, the potassium atom. The resulting photoelectron spectrum can then be regarded as the output, with the atom–laser interaction providing a functional input–output map. It is our goal to approximate this input–output map, and hence the atom's response to electric fields, by employing a neural network. Various trial pulses and the corresponding photoelectron spectra obtained from a simulation of the REMPI process in the potassium atom will be used to train the NN, which will then be employed to generalize beyond the training data set by predicting control landscapes. While the full multidimensional quantum control landscape as introduced by Rabitz *et al* [26–28] is generally not amenable to practical studies, lower dimensional subspaces—which we likewise refer to as control landscapes in the remainder of this paper—can be recorded by systematically varying few control parameters to change the input electric field. Experimentally, these landscapes, in which a control objective derived from observables is plotted as a function of selected parameters [18, 29–32], directly reflect the system's response to the different pulse shapes and give an indication about possible control mechanisms.

2. Simulation of physical system

The physical system we want the network to approximate consists of the two potassium bound states |4s⟩ and |4p⟩, strongly driven by a resonant shaped femtosecond laser pulse and weakly coupled to a continuum of ionic states, as depicted in figure 1 (centre). Resonant one-photon excitation and absorption of two further photons from the same laser field constitute a 1 + 2 photon REMPI process. As was shown recently [17], photoelectrons produced during the strong-field excitation of the atom directly map the non-perturbative dynamics of the neutral system. Thus, information on both the population and the quantum-mechanical phase of the bound states can be extracted from the photoelectron spectrum [22]. An intuitive physical picture of this scenario was devised in terms of SPODS. A description in the framework of dressed states is especially suited for this process, since ionization occurs simultaneously to excitation, and the dressed states, i.e., the eigenstates of the two-level system and the light field, are probed, rather than the bare atomic states. The splitting of the dressed-state eigenenergies (thick and dotted black lines in figure 1 (centre)), which is proportional to the laser field strength, is mapped into the photoelectron spectrum, which gives rise to the well-known Autler–Townes (AT) doublet [33].

Making use of the fact that the coupling among the two bound states is much stronger than the coupling of either bound state to the continuum, the numerical calculation of the photoionization process is divided into two steps. First, the strong-field interaction of the shaped laser pulse with the neutral system is treated by solving the time-dependent Schrödinger equation (TDSE) [34]

$$\mathrm{i}\hbar\frac{\mathrm{d}}{\mathrm{d}t}\begin{pmatrix}c_{4\mathrm{s}}\\ c_{4\mathrm{p}}\end{pmatrix}=-\frac{\hbar}{2}\begin{pmatrix}0 & \Omega(t)\\ \Omega^{*}(t) & 0\end{pmatrix}\begin{pmatrix}c_{4\mathrm{s}}\\ c_{4\mathrm{p}}\end{pmatrix} \tag{1}$$

in the interaction picture, applying the rotating-wave approximation (RWA) and using the short-time propagator method. Herein, $c_{4\mathrm{s}}$ and $c_{4\mathrm{p}}$ are the time-dependent probability amplitudes of the corresponding quantum states and $\Omega(t)$ denotes the complex Rabi frequency. Introducing the $4\mathrm{s}\rightarrow 4\mathrm{p}$ transition dipole moment (along the laser polarization) μ, the Rabi frequency is related to the laser electric field $E(t)$ by $\hbar\Omega(t)=\mu E(t)$.

In the second step, the two-photon ionization starting from the 4p state is evaluated in the framework of second-order perturbation theory. The final photoelectron amplitude then reads [36–39]

$$c(\omega_e)\propto\int_{-\infty}^{\infty}c_{4\mathrm{p}}(t)E^2(t)\,\mathrm{e}^{\mathrm{i}(\omega_e+\omega_{IP}-\omega_{4\mathrm{p}})t}\,\mathrm{d}t, \tag{2}$$

with $\hbar\omega_e$ being the kinetic excess energy of the emitted electron, $\hbar\omega_{IP}$ the potassium ionization potential and $\hbar\omega_{4\mathrm{p}}$ the eigenenergy of the 4p state.

Pulse shaping is carried out in the frequency domain, as summarized in [35]. To this end a bandwidth-limited 30 fs full-width at half-maximum (FWHM) Gaussian laser pulse with amplitude $A(\omega)$ is spectrally phase modulated, allowing for second- and third-order polynomial phase functions $\varphi(\omega)=\phi^{(n)}/n!(\omega-\omega_0)^n$, sinusoidal phase functions $\varphi(\omega)=A\sin[(\omega-\omega_0)\tau+\phi_0]$ as well as linear combinations of the form:

$$\varphi(\omega)=A\sin[(\omega-\omega_0)\tau+\phi_0]+\frac{\phi^{(2)}}{2}(\omega-\omega_0)^2. \tag{3}$$

The laser central frequency ω_0 coincides with the $4\mathrm{s}\rightarrow 4\mathrm{p}$ transition frequency. From the modulation function $\varphi(\omega)$ the modulated spectral electric field is calculated as

$$E(\omega)=A(\omega)\,\mathrm{e}^{-\mathrm{i}\varphi(\omega)} \tag{4}$$

and the temporal electric field is obtained via inverse Fourier transformation $E(t)=\mathcal{F}^{-1}[E(\omega)](t)$. The pulse energy was chosen such that the dressed states exhibit a maximum energy splitting of 210 meV in accordance with the experimental observations in [19].

3. Neural network

A NN consists of neurons, which are basically simple processors, connected to inputs, outputs and/or other neurons, and arranged in layers as depicted in figure 2. This network graph serves to illustrate the flow of information, and each symbol (connecting lines, neurons) stands for a certain mathematical operation. Information is treated in terms of real-valued numbers x_i that travel along connecting lines.

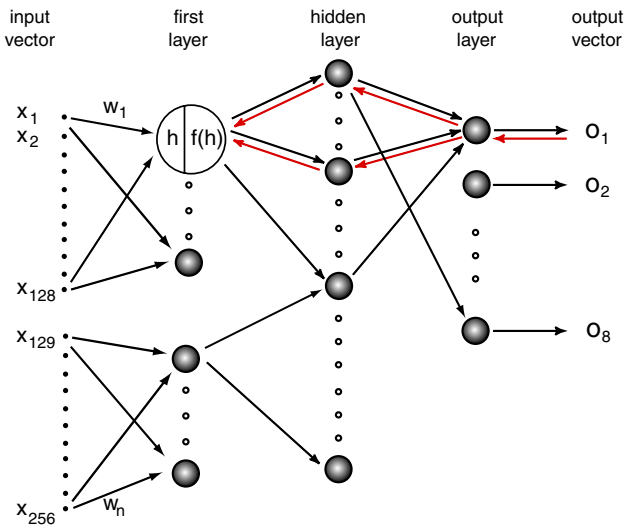

Figure 2. Schematic representation of the NN architecture and working principle. Neurons are depicted as spheres, and the flow of information and error correction is indicated by right-pointing and left-pointing arrows, respectively. If the weights w_i are adjusted correctly, the input vector is mapped onto the desired output vector by the underlying functional map.

For information processing, each number is multiplied with a weight w_i associated with this connection. All (weighted) information entering a neuron is then subjected to a so-called propagation function h, in our case the weighted sum is formed according to $h=\sum_i w_i x_i$. The resulting 'internal field' h is then inserted into the 'activation function' $f(h)$, in our case the error function,

$$f(h)=\frac{2}{\sqrt{\pi}}\int_0^h\mathrm{e}^{-t^2}\,\mathrm{d}t, \tag{5}$$

and the resulting output is transmitted to the receiving neurons or output channels in the same manner. The choice of this nonlinear activation function allows for varying output signal strength and saturation effects. It should be noted here that the use of nonlinear activation functions is one of the prerequisites for approximating nonlinear mappings, the other is the presence of at least one hidden layer of neurons, which is not directly connected to input and/or output nodes [14, 15]. We fulfil both requirements by employing the three-layer NN depicted in figure 2 and the activation function in equation (5).

As the process we want to approximate with a NN depends strongly on both the intensity and the phase of the electric field, it is sensible to use representations of the electric field, either in the frequency domain (equation (4)) or in the time domain, as inputs to the network.

The spectral phases are applied in the simulation of the potassium atom at 128 discrete frequencies, and hence the spectral electric field is evaluated at 128 points. We have tested spectral as well as temporal electric field representations, with the real and imaginary parts of the electric field as inputs to the NN, in total 256 variables (figures 1 (left) and 2 (left)). Examples of these different input representations are shown in figure 3. In figure 3(a) the spectral intensity (grey shaded) and phase (black line) are shown for the spectral phase $\varphi(\omega)=$

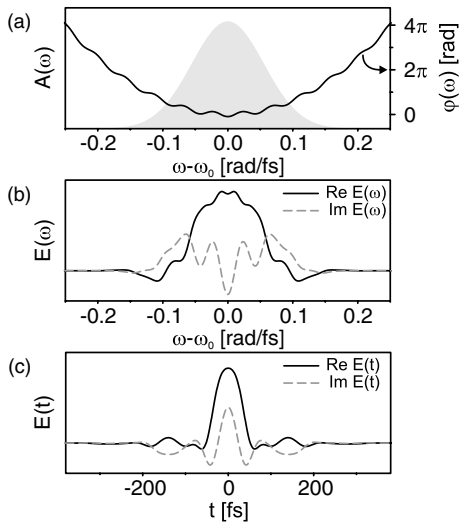

Figure 3. Different representations used for the electric field. (a) Spectral amplitude $A(\omega)$ (shaded background) and spectral modulation function $\varphi(\omega)$ for the modulation parameters $A = 0.3$ rad, $\tau = 140$ fs, $\phi_0 = -\pi/2$ and $\phi^{(2)} = 400\,\mathrm{fs}^2$ in (3). (b) Decomposition of the spectral electric field $E(\omega)$ into its real and imaginary parts. (c) Decomposition of the temporal electric field $E(t)$ into its real and imaginary parts.

$0.3\,\mathrm{rad}\sin[(\omega-\omega_0)140\,\mathrm{fs}-\pi/2]+\frac{1}{2}\times 400\,\mathrm{fs}^2(\omega-\omega_0)^2$. The real and imaginary parts of the resulting electric field are shown in the frequency (figure 3(b)) and the time (figure 3(c)) domain. In the following section, we examine how well the NN can be trained with these representations to simulate the photoelectron spectrum for different pulse shapes.

The first layer of neurons processes the real $(x_1 \ldots x_{128})$ and imaginary $(x_{129} \ldots x_{256})$ parts separately, each with eight neurons. The outputs of this first layer of neurons are then transferred to the hidden layer, consisting of 24 neurons. These are connected to the eight neurons of the output layer that deliver the photoelectron spectrum for eight photoelectron energy intervals (o_1 to o_8, confer figure 1) of equal width between 0.25 and 0.77 eV.

There are many options how the input, output and hidden neurons can be connected, and how the network parameters are then adjusted [14, 15]. For our purpose we have chosen a NN of the so-called feedforward-backpropagation type. Feedforward means that information is passed through the network in the forward direction only, i.e., from inputs towards outputs; there are no connections between neurons of the same layer or between layers other than one layer and the next one towards the output. Backpropagation describes how the most important parameters of the NN—the weights—are adjusted to the values suited for the function we want the network to approximate: The weights are initially assigned random values, which is a prerequisite for the successful performance of the NN; during a training process a large number of examples, consisting of input–output pairs, are presented to the NN. The input is entered into the network, processed as described above and delivers certain values o_j at the output nodes. These values are then compared to the correct, desired outputs. If there are any deviations, the error—or rather its correction—is then propagated backwards through the NN (from the output towards the input nodes) using the 'generalized delta rule' (for details see [14, 16]). This procedure is repeated until the overall error in the NN outputs for all training data sets cannot be further reduced.

4. Results and discussion

In order to provide a comprehensive set of data for training and testing the NN, photoelectron spectra for different classes of shaped laser pulses were generated, using the phase functions and the numeric model described in section 2. The polynomial phase parameters $\phi^{(n)}$ were varied within the following limits: from -2000 to $+2000$ fs^2 for quadratic phases, and from -15000 to $+15\,000$ fs^3 for cubic phases. For the sinusoidal phases the frequency τ was fixed to 140 fs and amplitudes A of $0.1, 0.2, \ldots, 0.5$ [rad] were used; the phase ϕ_0, which is the sine parameter the studied process is most sensitive to, was varied from 0 to 2π. In total, circa 5000 pulses and corresponding photoelectron spectra entered the training procedure: 1000 for second- and third-order modulation respectively and 630 for each value of the sine amplitude.

Simulated pulse shapes with either purely polynomial or sinusoidal phases and resulting photoelectron spectra were used for the training of the NN. The ability of the NN to learn the mapping of the shaped electric field onto the photoelectron spectrum from the training data set is shown in figure 4 for two representative classes of pulse shapes. The contour plots in the upper row show the photoelectron spectra resulting from the numeric model of section 2 for second-order spectral phases (left) and sinusoidal phases (right). The second row shows the corresponding photoelectron spectra generated by a NN with the spectral electric field $E(\omega)$ as input after the training is completed. In both cases, the agreement between the NN results and the exact results from the simulation is satisfactory, both qualitatively and quantitatively (compare figures 4(a) and (b) as well as figures 4(d) and (e)). The last row shows the photoelectron spectra generated by a NN with the temporal electric field $E(t)$ as input. Compared to the spectral input representation, the results are poor. While the photoelectron spectra for phases of second order (figure 4(c)) resemble qualitatively the expected results (figure 4(a)), the spectra for sinusoidal phases (figure 4(f)) show little variation depending on the phase parameter ϕ_0. Apparently, for this input representation, the minimization of the training error led to a network which always delivers the average spectrum. This can be rationalized by the fact that in the spectral representation all information is always contained in a limited frequency interval, whereas in the time domain relevant information is not *a priori* confined to a finite time interval. Moreover, even simple *spectral* structures such as a phase jump of π at the central frequency produce temporal fields which are difficult to be implemented numerically. In our case, however, undersampling of the input electric field was precluded by a careful choice of both time and frequency interval and resolution. Due to the above findings, the network with $E(\omega)$ as input was used for predicting the control landscapes in the

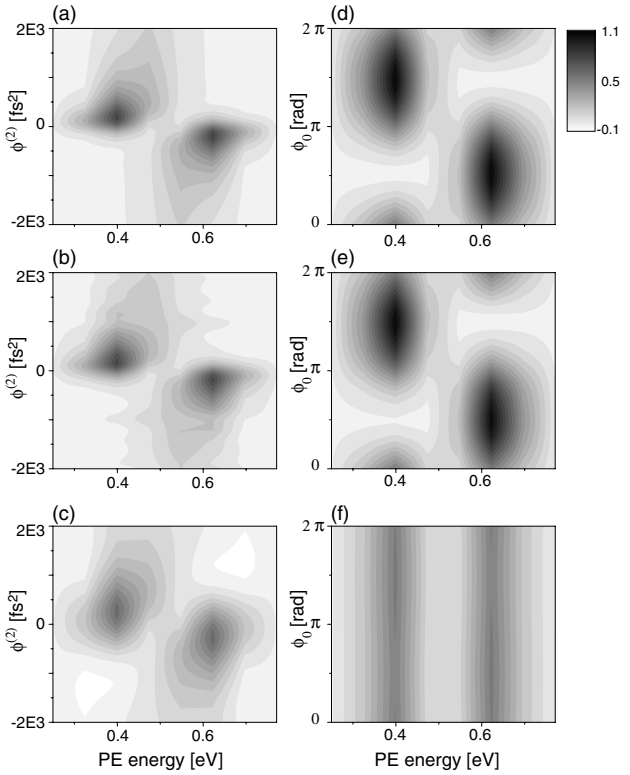

Figure 4. Contour plots of the photoelectron spectra for second-order spectral phases $\varphi(\omega) = \phi^{(2)}/2(\omega - \omega_0)^2$ (left column) and sinusoidal phases $\varphi(\omega) = 0.2\,\text{rad}\sin[(\omega - \omega_0)140\,\text{fs} + \phi_0]$ (right column). The top row shows the simulation. In the second row, results from the NN with $E(\omega)$ used as input are displayed. Results obtained from the NN when $E(t)$ is used as input are shown in the bottom row.

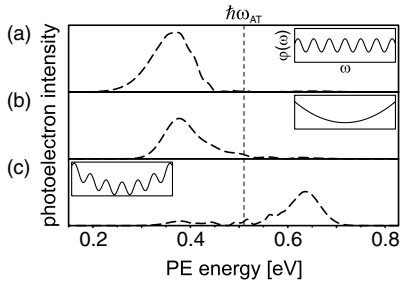

Figure 5. Selected photoelectron spectra corresponding to (a) sinusoidal phase modulation with parameters $A = 0.4$ rad, $\tau = 140$ fs and $\phi_0 = 1.02$ rad, (b) quadratic phase modulation with $\phi^{(2)} = 500\,\text{fs}^2$ and (c) a linear combination of these two (see equation (3)). The phase modulation functions $\varphi(\omega)$ are shown schematically in the insets and the energy $\hbar\omega_{AT}$ marks the centre of the AT doublet, separating slow from fast photoelectrons.

remainder of this work, as it is able to reproduce the training data accurately.

Ideally, one would hope that a network trained with purely polynomial and sinusoidal phases could be able to predict the outcome resulting from a linear combination of second-order and sinusoidal phases. However, this expectation turns out to be rather naive, given the complexity of the coherent strong-field dynamics involved. As was pointed out before, the physical process considered here is sensitive to virtually all details of the laser pulse such as the pulse energy, the pulse envelope, the instantaneous frequency and phase. Therefore—also taking into account the nonlinearity of the photoionization—a simple interdependence of parameters is not to be expected. The mutual interdependence of chirps and phase jumps is illustrated in figure 5, where exemplary photoelectron spectra from (a) a purely sinusoidal modulation, (b) a purely quadratic modulation and (c) a linear combination of both types of modulation are compared. While both the sinusoidal and the quadratic modulations alone lead to the exclusive production of slow photoelectrons, i.e., the low energetic AT component, this picture is completely inverted in the case of the combined modulation. Now the production of fast electrons is favoured and only the high energetic AT component shows up in the spectrum. This reflects the fact that in general the shape of the AT doublet resulting from a combined phase modulation cannot be decomposed into contributions of each elementary modulation, but arises from a complex interplay of the modulation parameters, exemplifying the quantum-mechanical nature of the underlying effects. Taking into account this complexity of the strong-field-induced dynamics it is not surprising that additional information is needed for the NN to accurately predict two-dimensional control landscapes. Shaped pulses resulting from a linear combination of second-order and sinusoidal phases were used to generate such control landscapes. The contour plots of these control landscapes show the total photoelectron count belonging to the high energetic component of the Autler–Townes doublet (from 0.51 to 0.77 eV in figure 5) as a function of second-order phase (from -1000 to $+1000$ fs^2) and the varied sinusoidal phase parameter, here ϕ_0 (from 0 to 2π), for varying sine amplitude A and τ again fixed at 140 fs.

It turned out that after inclusion of few control landscapes into the training data set (namely those with sine-parameters $A = 0.2$ and $A = 0.4$, shown in figures 6(a) and (b)), the network was quite capable of interpolating and extrapolating to the control landscapes which were not included in the training data. In figures 6(c)–(h) the control landscapes are depicted for sine-parameters $A = 0.1$, $A = 0.3$ and $A = 0.5$, which show the intensity of fast photoelectrons in dependence on the applied second-order phase coefficient $\phi^{(2)}$ and the sinusoidal phase parameter ϕ_0. The exact control landscapes from the numeric model are shown in the second row, the corresponding control landscapes approximated by the network in the bottom row. Again, the agreement between the exact results and the network approximation is convincing both qualitatively and quantitatively. Apparently, the coherent dynamics induced by shaped electromagnetic fields that were not included in the training data set can be predicted by the network, provided that the phase modulations of these new fields resemble at least to some extent the phase modulations encountered during the training process. It should be noted that the NN interpolation and extrapolation for pulses that were previously 'unknown' to the NN (figures 6 (c)–(h)) works even if the landscapes differ significantly from those used during the training process (figures 6(a), (b)).

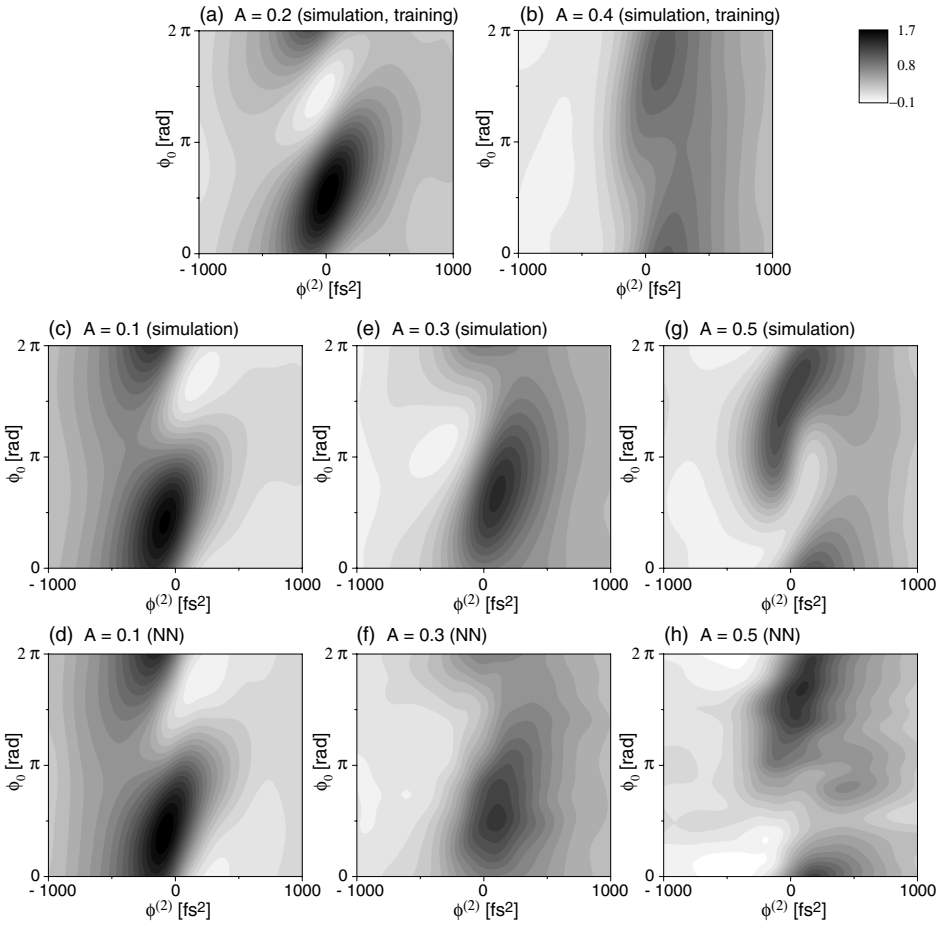

Figure 6. Control landscapes—intensity of fast photoelectrons (cf figure 5) as a function of second-order phase $\phi^{(2)}$ (from −1000 to +1000 fs^2) and the varied sinusoidal phase parameter, here ϕ_0 (from 0 to 2π), with τ fixed at 140 fs. In the top row, the exact results of the numeric model that were used for the training process are shown for (a) $A = 0.2$ and (b) $A = 0.4$. The NN is then employed for interpolating the control landscapes for different values of A. The simulated landscapes are shown in the second row, the corresponding NN predictions in the bottom row for ((c) and (d)) $A = 0.1$, ((e) and (f)) $A = 0.3$ and ((g) and (h)) $A = 0.5$.

5. Conclusions

We employed a neural network (NN) to predict photoelectron spectra from resonant strong-field ionization of potassium atoms. The application of NNs for the automated generation of input-output maps of physical processes has been very successful for comparatively simple systems, such as second-harmonic generation (SHG) or molecular fluorescence yield [16]. Here, a more complex situation was examined, where the outcome of the light-driven process depends critically on all details of the laser field. It turned out that the amount of data required for the training strongly increase with the complexity of the correlations which are to be modelled. Under such conditions, extrapolation to regions of the parameter space which were not covered at all by the training data is still a challenge. However, reproduction of the training data worked excellent, provided that an appropriate representation of the input fields was used. Moreover, when taking two-dimensional data the coherent strong-field dynamics could be predicted by the NN for laser pulse shapes not included in the training data set.

As a next step, it would be interesting to study the applicability of NNs to the field of nonlinear spectroscopy [40], in order to see if a NN can model the response function from one spectroscopy technique (e.g. transient grating or photon echo), and if this response function in turn could be used to predict the outcome of different spectroscopy experiments based on a nonlinearity of the same order.

Acknowledgments

The Würzburg group was supported by the Emmy Noether Program (DFG). The Kassel group appreciates support via DFG Normalprogramm.

References

[1] Weiner A M 2000 *Rev. Sci. Instrum.* **71** 1929
[2] Bardeen C J, Yakovlev V V, Wilson K R, Carpenter S D, Weber P M and Warren W S 1997 *Chem. Phys. Lett.* **280** 151
[3] Assion A, Baumert T, Bergt M, Brixner T, Kiefer B, Seyfried V, Strehle M and Gerber G 1998 *Science* **282** 919

[4] Brixner T, Damrauer N H, Niklaus P and Gerber G 2001 *Nature* **414** 57
[5] Levis R J, Menkir G M and Rabitz H 2001 *Science* **292** 709
[6] Herek J L, Wohlleben W, Cogdell R, Zeidler D and Motzkus M 2002 *Nature* **417** 533
[7] Daniel C, Full J, González L, Lupulescu C, Manz J, Merli A, Vajda Š and Wöste L 2003 *Science* **299** 536
[8] Brixner T and Gerber G 2003 *ChemPhysChem.* **4** 418
[9] Brixner T, Krampert G, Pfeifer T, Selle R, Gerber G, Wollenhaupt M, Graefe O, Horn C, Liese D and Baumert T 2004 *Phys. Rev. Lett.* **92** 208301
[10] Vogt G, Krampert G, Niklaus P, Nürnberger P and Gerber G 2005 *Phys. Rev. Lett.* **94** 068305
[11] Wollenhaupt M, Präkelt A, Sarpe-Tudoran C, Liese D and Baumert T 2005 *J. Opt. B: Quantum Semiclass. Opt.* **7** S270
[12] Horn C, Wollenhaupt M, Krug M, Baumert T, de Nalda R and Bañares L 2006 *Phys. Rev.* A **73** 031401
[13] Nürnberger P, Vogt G, Brixner T and Gerber G 2007 *Phys. Chem. Chem. Phys.* **9** 2470
[14] Hertz J, Krogh A and Palmer R 1991 *Introduction to the Theory of Neural Computation* (New York: Perseus Books Group)
[15] Freeman J A and Skapura D M 1991 *Neural Networks: Algorithms, Applications, and Programming Techniques (Computation and Neural Systems Series)* (Redwood City, CA: Addison-Wesley Longman Publishing Co.)
[16] Selle R, Vogt G, Brixner T, Gerber G, Metzler R and Kinzel W 2007 *Phys. Rev.* A **76** 023810
[17] Wollenhaupt M, Engel V and Baumert T 2005 *Ann. Rev. Phys. Chem.* **56** 25
[18] Wollenhaupt M, Präkelt A, Sarpe-Tudoran C, Liese D and Baumert T 2005 *J. Mod. Opt.* **52** 2187
[19] Wollenhaupt M, Liese D, Präkelt A, Sarpe-Tudoran C and Baumert T 2006 *Chem. Phys. Lett.* **419** 184
[20] Wollenhaupt M, Präkelt A, Sarpe-Tudoran C, Liese D and Baumert T 2006 *Appl. Phys.* B **82** 183
[21] Wollenhaupt M, Präkelt A, Sarpe-Tudoran C, Liese D, Bayer T and Baumert T 2006 *Phys. Rev.* A **73** 063409
[22] Wollenhaupt M, Assion A, Bazhan O, Horn C, Liese D, Sarpe-Tudoran C, Winter M and Baumert T 2003 *Phys. Rev.* A **68** 015401
[23] Vitanov N V, Halfmann T, Shore B W and Bergmann K 2001 *Ann. Rev. Phys. Chem.* **52** 763
[24] Sleva E T, Xavier I M Jr and Zewail A H 1986 *J. Opt. Soc. Am.* B **3** 483
[25] Kosloff R, Hammerich A D and Tannor D 1992 *Phys. Rev. Lett.* **69** 2172
[26] Rabitz H A, Hsieh M M and Rosenthal C M 2004 *Science* **303** 1998
[27] Rabitz H A, Hsieh M and Rosenthal C 2006 *J. Chem. Phys.* **124** 204107
[28] Rothman A, Ho T S and Rabitz H 2006 *Phys. Rev.* A **73** 053401
[29] Langhojer F, Cardoza D, Baertschy M and Weinacht T 2005 *J. Chem. Phys.* **122** 014102
[30] Cardoza D, Trallero-Herrero C, Langhojer F, Rabitz H and Weinacht T 2005 *J. Chem. Phys.* **122** 124306
[31] Vogt G, Nürnberger P, Selle R, Dimler F, Brixner T and Gerber G 2006 *Phys. Rev.* A 033413
[32] Shane J C, Lozovoy V V and Dantus M 2006 *J. Phys. Chem.* A **110** 11388
[33] Autler S H and Townes C H 1955 *Phys. Rev.* **100** 703
[34] Shore B W 1990 *Theory of Coherent Atomic Excitation* vol 1 (New York: Wiley)
[35] Wollenhaupt M, Assion A and Baumert T 2007 *Springer Handbook of Lasers and Optics* ed F Träger (New York: Springer) chapter 12
[36] Bebb H H and Gold A 1966 *Phys. Rev.* **143** 1
[37] Meier C and Engel V 1994 *Phys. Rev. Lett.* **73** 3207
[38] Meshulach D and Silberberg Y 1998 *Nature* **396** 239
[39] Meshulach D and Silberberg Y 1999 *Phys. Rev.* A **60** 1287
[40] Mukamel S 1995 *Principles of Nonlinear Optical Spectroscopy* (New York: Oxford University Press)